

In-Situ Analysis of Corrosion Products in Molten Salt: X-ray Absorption Reveals Both Ionic and Metallic Species

Sean Fayfar, Guiqiu Zheng, David Sprouster, Matthew S. J. Marshall, Eli Stavitski, Denis Leshchey, and Boris Khaykovich*



Cite This: *ACS Omega* 2023, 8, 24673–24679



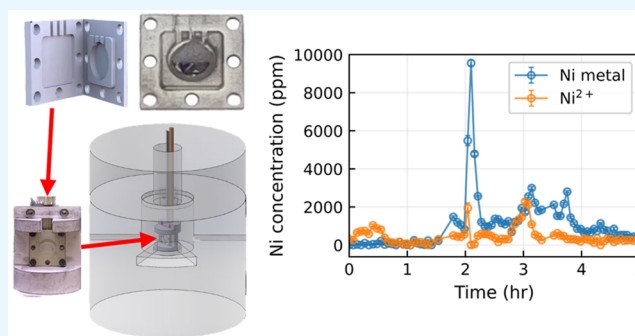
Read Online

ACCESS |

Metrics & More

Article Recommendations

ABSTRACT: Understanding and controlling the chemical processes between molten salts and alloys is vital for the safe operation of molten-salt nuclear reactors. Corrosion processes in molten salts are highly dependent on the redox potential of the solution that changes with the presence of fission and corrosion processes, and as such, reactor designers develop electrochemical methods to monitor the salt. However, electrochemical techniques rely on the deconvolution of broad peaks, a process that may be imprecise in the presence of multiple species that emerge during reactor operation. Here, we describe in situ measurements of the concentration and chemical state of corrosion products in molten FLiNaK (eutectic mixture of LiF–NaK–KF) by high-resolution X-ray absorption spectroscopy. We placed a NiCr foil in molten FLiNaK and found the presence of both Ni²⁺ ions and metallic Ni in the melt, which we attribute to the foil disintegration due to Cr dealloying.



1. INTRODUCTION

Molten-salt reactor (MSR) concepts are advanced nuclear reactor designs that benefit from lower operating pressures and higher heat transfer efficiency compared with traditional water-cooled designs.^{1–4} Molten salts are utilized not only as a coolant fluid but also as a carrier of the fissile material. These applications require online monitoring of salt chemistry for a number of reasons. First, molten alkali halides become corrosive in the presence of impurities. Second, in the presence of corrosion and fission products, the salts might change their thermophysical and thermochemical properties, leading to suboptimal reactor operation conditions, stress-corrosion cracking,^{5,6} or undesired plating on metal parts.^{7–9} To understand and mitigate changes in the salt during operation, detailed information about the concentration of corrosion and fission products is necessary and should be measured in situ. Electrochemical techniques are proposed for that task. For example, the redox potential of salt could be monitored and controlled to mitigate the effects of impurities and to measure the efficacy of salt-cleaning procedures,^{10–14} but the redox potential is affected by all impurities in the mixture. While electrochemical techniques are element specific,^{15,16} they are relatively low-resolution methods that produce broad element-specific peaks that overlap in multicomponent solutions.¹⁷ By comparison, high-resolution X-ray absorption spectroscopy (XAS) is an extremely sensitive atom-specific method. It is

sensitive to the oxidation state of ions and their local environment at concentrations down to a few ppm, and it can also be used to measure the concentration of impurities with a detection limit of better than 10 ppm.^{18,19} Since XAS is likely impractical to implement in a working reactor, these studies should be conducted in the lab. To combine the strengths of both methods, we are developing sample cells to perform both XAS and electrochemical measurements of molten salts simultaneously. This combination will reinforce standard electrochemical methods and provide a rich data stream for modeling. Here, we report the first step in this direction by using XAS to quantify the corrosion product Ni produced by a NiCr foil immersed in a molten fluoride salt.

In situ measurements of molten salts pose difficult challenges. For example, optical characterization techniques such as Raman, UV, and IR spectroscopy typically require cells to be made out of transparent materials such as glass and quartz. These materials degrade when in contact with molten fluorides, which chemically attack them.²⁰ As such, placing

Received: May 17, 2023

Accepted: June 9, 2023

Published: June 29, 2023



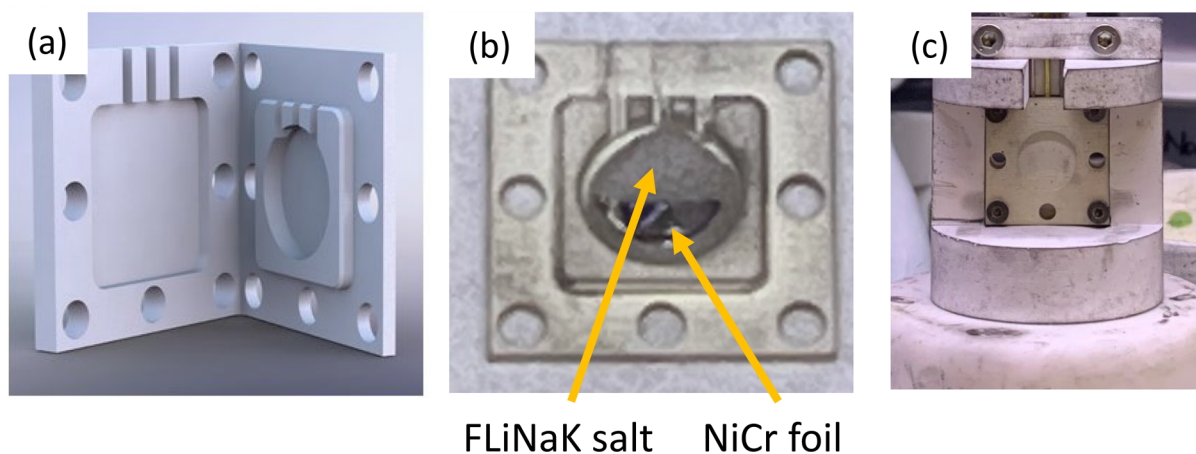


Figure 1. Pyrolytic boron nitride cell containing FLiNaK salt and a NiCr foil designed for XAS fluorescence measurements in a furnace. (a) 3D design of the boron nitride cell including two parts. (b) FLiNaK salt and NiCr foil loaded into the boron nitride cell. (c) Assembled cell placed in a holder and then into the furnace.

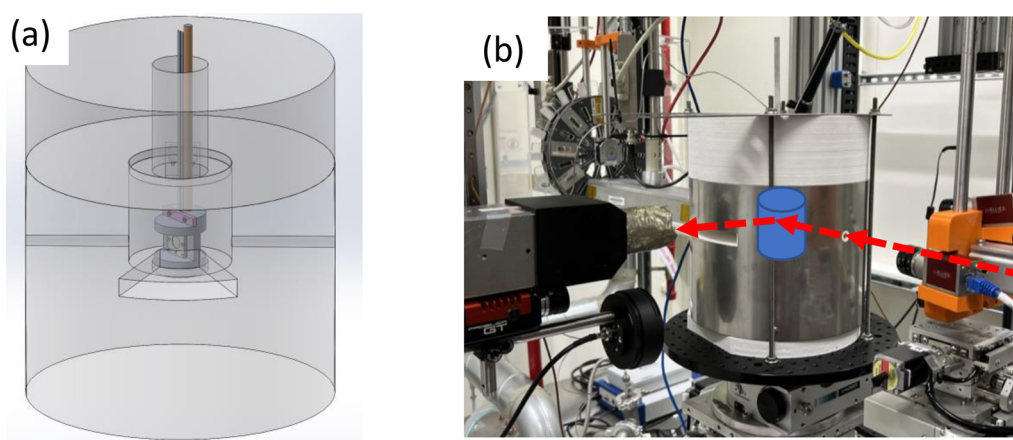


Figure 2. (a) 3D design of the furnace built for XAS, and (b) the furnace installed at the ISS beamline. The BN cell sits in a central chamber of the furnace with small holes for the incoming and transmitted beam. There is a larger window in the furnace for the fluorescence signal. A thermocouple is placed through the top to monitor the temperature within the furnace.

molten fluoride salts in containers made from graphite,^{21–23} glassy carbon,²⁴ boron nitride,^{25–27} and metal alloys^{28–32} prevents the salt from degrading and penetrating the container. While ceramics are compatible with XAS, they are difficult to machine and seal; on the other hand, metals are not compatible with XAS and can themselves contribute corrosion products during measurements. Therefore, we are developing an experimental apparatus for probing molten fluorides using a pyrolytic boron nitride (BN) cell that was optimized for use with XAS. Several new designs of electrochemical cells have been developed with the goal of studying the corrosion process,^{24,33–35} and we aim to augment these developments starting from an XAS perspective. Our sample cell was designed to perform quantitative XAS measurements on fluoride-based salts. This apparatus, when employed at XAS facilities, can be utilized to determine the time evolution of important impurities in the salt at the microscopic level across relevant time scales (minutes-to-hours) and temperatures (460 to 750 °C) pertinent to MSR technology.

We present our results of monitoring corrosion products that leached into the molten salt from a NiCr foil immersed in it. In our experiments, the foil was placed in molten FLiNaK, the eutectic mixture of LiF–NaK–KF. We demonstrated detailed measurements of the quantity and chemical state of Ni

by XAS. We calibrated the XAS intensity using salt mixtures with known concentrations of Ni, and we deduced the concentrations of both Ni²⁺ and metallic Ni as a function of corrosion time at MSR operating temperatures. Furthermore, we measured the spatial distribution of Ni in the salt samples after quenching. We concluded that the unexpected Ni metal signal is from grains of foil liberated due to moisture and oxygen within the salt, increasing the corrosion rate.

We stipulate that the presence of a high concentration of Ni in the salt is likely caused by the oxygen or moisture impurities that penetrated thin membranes of the sample cells. Measuring correlations between the concentration of oxygen/moisture and corrosion products is beyond the scope of this work, which is devoted to high-sensitivity measurements of corrosion products. However, the next step of this research is to control and measure the redox potential of the salt simultaneously with XAS measurements. Most importantly, some ingress of oxygen and moisture into operating MSR salt is expected, and it is important to understand their effects. Our method could provide an avenue of such exploration.

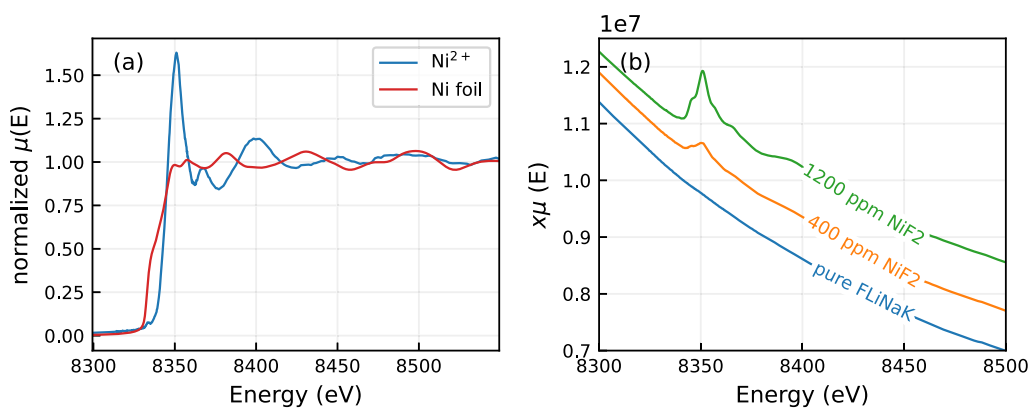


Figure 3. (a) XANES spectra of Ni^{2+} and Ni foil normalized for comparison. (b) XANES results of the Ni K-edge of FLiNaK with varying concentrations of NiF_2 . The step size of the XANES measurement corresponds to the concentration of Ni in the sample. The vertical heights are shifted for clarity.

2. METHODS

2.1. Sample Preparations and Measurement Apparatus.

FLiNaK, the eutectic mixture of LiF–NaK–KF, is a model fluoride salt that was chosen because of the relative ease of handling, well-known characteristics, and previous corrosion studies.^{23,36,37} Its composition is a mixture of 46.5 mol % LiF, 11.5 mol % NaF, and 42 mol % KF salt. All three salts are high-purity chemicals procured from Alfa Aesar. Purified FLiNaK was prepared in a laboratory glovebox by drying, premixing, and melting of component salts in cleaned and dried glassy-carbon containers (procured from HTW, Germany). The salt was checked for metallic impurities, but moisture analysis was not performed since the focus of this study is not to prevent corrosion but to monitor it.³⁸ The Ni80/Cr20 foil with a thickness of 0.005 mm was procured from Goodfellow Cambridge Limited. FLiNaK salt specimens with known concentrations of NiF_2 were prepared by mixing NiF_2 powder (anhydrous, 99%, Strem Chemicals Inc.) with the above FLiNaK salt in a certain ratio in glassy carbon crucibles. The powders underwent several melting–freezing–grinding cycles to fabricate well-mixed samples of FLiNaK– NiF_2 with 400 ppm and 1200 ppm of NiF_2 .

To contain the salt, we designed a cell made from a pyrolytic boron nitride (BN) that is capable of withstanding both the corrosive nature of the salt and the high-temperature sample environment of interest. This specifically designed boron nitride cell is composed of two parts: the bottom salt compartment and the top cover; the cell is shown in Figure 1a. Molten salt can be sealed in this cell by bolting the four corners using stainless steel bolts and nuts. (The cell can accommodate openings for the electrodes in the future.) We note that thin BN membranes (0.5 mm thick) can allow for moisture and air to penetrate into the cell. To minimize the amount of oxygen and moisture, an Ar gas line placed at the top of the furnace was flowing for the duration of the experiment. The BN cell is placed in a custom ceramic furnace capable of containing the sample apparatus with windows for both transmission and fluorescence mode XAS, as shown in Figure 2.

2.2. X-ray Absorption Spectroscopy. Fluorescence-mode X-ray absorption near-edge structure (XANES) and extended X-ray absorption fine structure (EXAFS) measurements were performed at the Inner Shell Spectroscopy (ISS) beamline at the National Synchrotron Light Source II (NSLS-

II).³⁹ XANES and EXAFS measurements were performed on specimens at the Ni K-edge (8.333 keV) (Figure 3). Spectra were recorded by using a four-element silicon drift detector (SDD) and a total fluorescence yield detector (PIPS diode). Data were collected to a photoelectron wavenumber (k) value of $14^\circ \text{ \AA}^{-1}$. For energy calibration, a Ni reference foil was measured in transmission mode. Background subtraction, spectra alignment, and normalization of the XANES and EXAFS data were performed with ATHENA⁴⁰ and Larch.⁴¹ Dedicated Python scripts were developed to visualize the processed data and perform quantitative concentration analyses of the XAS spectra.

The raw intensity of the step size in XANES is directly related to the amount (or concentration) of the element in a sample. The raw XANES signal can then be calibrated with known samples to determine a linear relationship between the step intensity and the concentration of an absorbing element.^{18,19} As such, the two calibration samples and pure FLiNaK were measured at room temperature with the BN cell cover placed in front of the salt to match the environment of the salt in the BN cell. The BN cell cover was placed at 45° angles with respect to the incoming beam to minimize the path that the X-ray beam travels through the BN cover.

The in situ XAS corrosion measurements were performed on molten FLiNaK in the BN cell with a metal foil of Ni80–Cr20 placed toward the bottom. The foils were 0.005 mm thick and approximately 9 mm wide coupons in the shape of a half moon (see Figure 1b). The BN cell was placed inside an alumina holder with a vertical shim for ease of placement and alignment at the top of the heating furnace (see Figures 1c and 2a).

We performed two corrosion experiments on molten FLiNaK. The first experiment utilized a precursor heater that used conduction to heat the sample and a closed BN cell. The second experiment used the furnace built for an XAS beamline, shown in Figure 2. The sample was placed at a 45° angle with respect to the incoming beam, and the detector was placed perpendicular to the incoming beam. Both samples were heated at approximately $10^\circ \text{C}/\text{min}$ until reaching 500 and 650°C , respectively. The X-ray beam was placed approximately 3 mm and 4 mm from the foil in each of the experiments, respectively. Once the corrosion measurements were completed, the samples were quenched to room temperature. The BN cell from the first experiment was vertically scanned after being cooled to investigate the distribution of Ni within the cell. The horizontal position of the X-ray beam was likely not

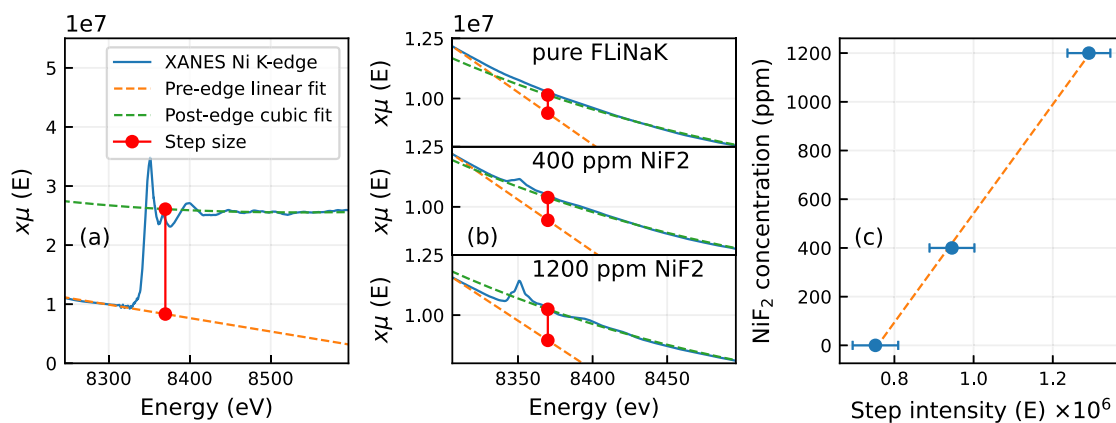


Figure 4. Step size fitting results of XANES spectra. (a) XANES spectra of the Ni K-edge with fits to the pre- and post-edge and the calculated step size. (b) The fits to the spectra with known concentrations of NiF₂. (c) Fit correlating the step size with NiF₂ concentration.

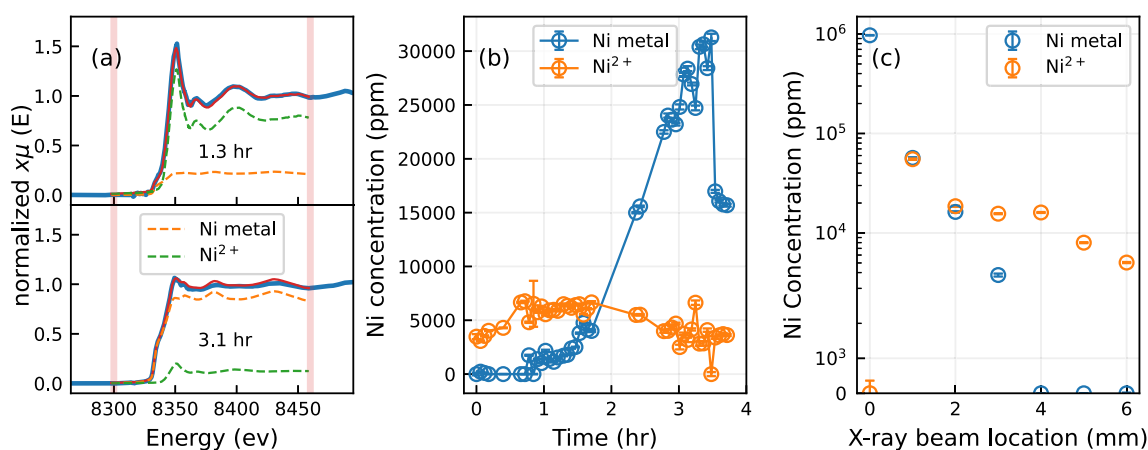


Figure 5. XANES results of the Ni K-edge of molten FLiNaK at 500 °C over a period of 3.75 h. (a) Two of the spectra analyzed with LCA using a Ni metal spectra and a Ni²⁺ spectra; the fitting bounds are shown as red vertical lines. (b) The concentration of Ni ions calculated from the XANES step size. (c) The spatial distribution of Ni concentrations postcorrosion at room temperature where 0 mm corresponds to the location of the metal foil.

at the same location as the corrosion measurements due to the cell and salt movement during quenching.

2.3. Quantitative Analysis of XANES. To monitor the concentration of Ni corroded into the molten salt, the height of the edge step of the Ni K-edge needed to be determined from the XANES spectra. We fitted the pre-edge with a linear function and the post-edge with a cubic function. The edge step size is the difference in intensity between the refinements at a chosen point in the energy spectrum; the same point in energy was used to compare different spectra. This procedure is shown in Figure 4a with fits to the pre- and post-edge regions to calculate the size of the step.

To correlate the XANES Ni-edge step size with the concentration of Ni ions in the salt, we calculated the step sizes of the calibration samples. The step size relates linearly with the concentration of Ni in the sample.^{18,19} The fits of the step size correlated to the NiF₂ concentration are shown in Figures 4b and 4c. Uncertainties in the NiF₂ concentration are determined from the uncertainties calculated from the fitting procedure for the pre- and post-edge regions.

Since XAS captures both the concentration of materials in the step edge size and the oxidation state in the fine structure, we can separate out the contribution of metallic Ni and Ni²⁺. Both oxidation states can exist simultaneously in the melt, and their respective spectra add together, creating a linear

combination of the components. We made use of Larch⁴¹ Python modules to perform the linear combination analysis (LCA) on all of the corrosion measurements. The standards for each of the oxidation states of Ni are shown in Figure 3a. The fitting region and parameters for LCA were kept consistent for each of the spectra. An example of the LCA result is displayed in Figure 5a with the fits shown as a red line.

3. RESULTS

The results for the calibration measurements are shown in Figure 4. The pre- and post-edges are fit, and the resulting step edge was calculated at a single energy value. Since the concentrations relate linearly with the step size,^{18,19} we fit the results with the orange dashed line. This fitting result was used to calculate the total Ni concentration during corrosion measurements. LCA was then used to separate metallic Ni from Ni²⁺.

The results of the first corrosion measurements are displayed in Figure 5. The XANES spectra showed a clear increase in intensity during the duration of the 4 h, but after LCA, we determined that the Ni²⁺ concentration plateaued. Metallic Ni increased significantly after approximately 2 h and decreased toward the end of the experiment. The metallic Ni appeared to be mobile in the molten salt by moving into the X-ray beam and then moving out of it. Note that the concentration of Ni²⁺

did not start out at zero due to prebeamtime baking during sample preparation, although the concentration of metallic Ni did start at zero and required significantly more time at high temperature before appearing in the melt.

Postcorrosion XANES spectra collected along the vertical direction of the BN cell were measured to determine a snapshot of the spatial distribution of Ni within the salt. The spectra as a function of the distance from the foil are shown in Figure 5c. To avoid time-dependent changes in concentration during measurements, the spatial scans were done at room temperature after high-temperature corrosion experiments were completed. The Ni²⁺ valence state is apparent from the XANES measurements at the distances away from the foil location, and the spectrum at 0 mm is purely metallic, as expected. The concentration at the foil (0 mm) should be 10⁶ ppm, and we calculated it to be 9.7(6) × 10⁵ ppm, which validates the accuracy of the procedure. A concentration gradient within the salt is apparent on a log–linear scale. We found that the spatial profiles of both Ni²⁺ and Ni⁰ concentrations cannot be fitted by a simple diffusion equation. We note that in Figure 5c the concentration of Ni²⁺ at 3 mm distance from the foil is much larger than that in Figure 5b. This is likely caused by the slight variation in horizontal position of the X-ray beam placement during measurements the following day and the salt movement during quenching. Furthermore, there is a small depth component to the salt that could lead to small variations.

This first corrosion experiment demonstrated that the custom BN cells were sufficiently transparent for XAS measurements to capture the valence state and concentration of corroded Ni ions while containing the salt at elevated temperatures. The BN cells both withstood the extreme temperatures within the furnace and held the salt without leakage. XAS captured the Ni concentration with enough temporal resolution to precisely track the corrosion products entering the melt.

The results from the second experiment and the Ni concentrations calculated from the XANES measurements are presented in Figure 6. The concentration of corroded Ni within the salt still did not follow a clear trend but, rather, peaked in certain regions and then decreased again. The XANES spectra in this experiment, similar to the previous ones, detected the presence of Ni²⁺ and metallic Ni (see Figure 6a). The metallic Ni XANES spectra were obvious at the

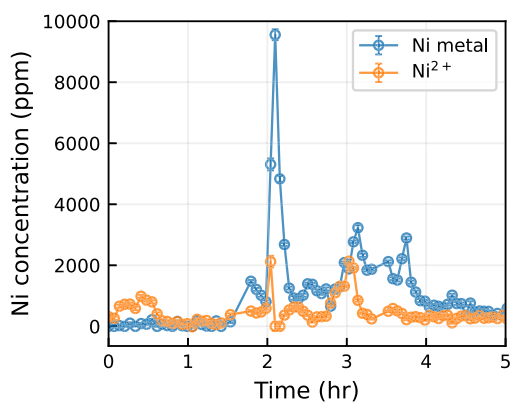


Figure 6. Results of the Ni K-edge XANES spectra at 650 °C over a period of 5 h. The concentration of Ni ions was calculated from the XANES step size.

locations of the peaks (2 and 3 h) in Figure 6a. This behavior is suggestive that the extreme environment caused small pieces/grains of the foil to be liberated from the foil and subsequently move throughout the melt. This is potentially related to the grain boundary attack described by Olson et al.²³ and Liu et al.⁴² The concentration of Ni²⁺ also spiked in unison with the metallic Ni peaks, suggesting that the metallic Ni pieces carry large Ni²⁺ concentration gradients with them.

4. DISCUSSION

The two experiments described above were made from the same materials in similar conditions. They show similar behavior, with some differences in detail. The first experiment showed an initial increase in Ni²⁺ concentration that stabilized and remained nearly constant for the remainder of the experiment. The concentration of Ni metal increased drastically after 2 h and then decreased toward the end. This suggests that very small pieces of foil were transported through the beam. The second experiment showed a relatively small and basically constant concentration of Ni²⁺ with occasional spikes in the Ni metal signal. The explanation for the lower and more constant Ni²⁺ concentration and more chaotic Ni metal concentration in the second experiment lies in the difference in the external conditions. The second experiment maintained a significantly higher temperature, which contributed to the metallic grains moving more quickly through the melt. Furthermore, the X-ray beam was placed farther from the foil in the second experiment, causing lower concentrations and smaller pieces of Ni metal to reach the beam. Nonetheless, we do not expect the experiments to match exactly since in each case the foil placement might move slightly within the melt and break apart in unique ways. Interestingly, both experiments had nearly zero metallic Ni until approximately 1.5 h had passed. This technique successfully quantified the corrosion products entering the melt by using XAS.

The corrosion of the foil was accelerated by the penetration of oxygen and moisture through the thin BN membrane from the external environment. Without the addition of oxygen and moisture, the concentrations of Ni²⁺ and Ni⁰ would have been much lower. Although an effort was made to shield the cells from the environment by flowing Ar gas into the furnace, oxygen and moisture did enter the salt. However, it does not invalidate our conclusions, as the scope of this study focused on monitoring corrosion products rather than preventing or controlling corrosion. Future studies are planned to combine electrochemical monitoring of the redox potential with XAS measurements that correlate the corrosion rate with the redox potential of the salt. These measurements require a more thorough control of the impurities within the salt. The use of electrochemical measurements will be potentially helpful in elucidating the causes of the large concentration variations we find between experiments.

One possible explanation of the presence of a Ni metal signal in these experiments is due to a radiation-induced reduction of Ni²⁺ to Ni⁰.^{43,44} While this might have been a contributing factor in our experiments, it was not the dominant source of metallic Ni for a few reasons. First, the fluoride salt was contained in a BN cell rather than quartz, which attenuated the X-ray beam intensity significantly and reduced the radiation dose. Second, we see in Figure 5c the metallic Ni concentration gradient that emanates directly from the NiCr foil and does not show a peak located at the X-ray beam location (3 mm). Lastly, the concentration of Ni metal in our

experiments is highly dynamic, with peaks caused by metal pieces moving through the beam rather than a steady increase that would be caused by the static beam placement. Therefore, we propose an alternative explanation that small Ni-rich grains were liberated from the foil due to the dissolution of Cr. Previous X-ray tomography and quasi in situ TEM observations of NiCr wires in molten KCl–MgCl₂ showed dealloying, grain boundary attacks, and salt penetration in cracks and pores.^{42,45,46} Such dealloying leaves behind a spongelike structure of Ni-rich grains that would easily detach into the solution. When caught in the X-ray beam, these pieces resulted in the dramatic spikes in Ni metal fluorescence shown in Figures 5b and 6. As expected, there is a coincident increase in Ni²⁺ concentration due to some dissolution of ions from metal pieces.

5. CONCLUSIONS

While the results for the corrosion processes varied slightly between experiments, in situ XAS proved to be a promising technique to investigate corrosion products produced by the interaction of molten salts and metals. Each experiment had slight variations in the conditions in the cell, but XANES captured the local Ni concentration and charge state in each case. The small X-ray beam probes the melt near the interface between the salt and foil, where the corrosion process occurs. XANES measurements captured and quantified the chemical state of Ni in the salt and provided an avenue to study not only the rate of corrosion directly next to the foil but also the diffusion or convection that occurs within the mixture. Combining the precise quantification of XAS with electrochemical techniques in future work will provide a method to elucidate the low-resolution peaks that are vital for monitoring of MSRs during operation. This work is a step toward these developments.

AUTHOR INFORMATION

Corresponding Author

Boris Khaykovich – Nuclear Reactor Laboratory, Massachusetts Institute of Technology, Cambridge, Massachusetts 02139, United States; orcid.org/0000-0002-9490-2771; Email: bkh@mit.edu

Authors

- Sean Fayfar** – Nuclear Reactor Laboratory, Massachusetts Institute of Technology, Cambridge, Massachusetts 02139, United States; orcid.org/0000-0002-3097-0054
- Guiqiu Zheng** – Nuclear Reactor Laboratory, Massachusetts Institute of Technology, Cambridge, Massachusetts 02139, United States
- David Sprouster** – Department of Materials Science and Chemical Engineering, Stony Brook University, Stony Brook, New York 11784, United States; Nuclear Reactor Laboratory, Massachusetts Institute of Technology, Cambridge, Massachusetts 02139, United States; orcid.org/0000-0002-2689-0721
- Matthew S. J. Marshall** – RMD Inc., Watertown, Massachusetts 02472, United States
- Eli Stavitski** – National Synchrotron Light Source II, Brookhaven National Laboratory, Upton, New York 11973, United States
- Denis Leshchev** – National Synchrotron Light Source II, Brookhaven National Laboratory, Upton, New York 11973, United States; orcid.org/0000-0002-8049-3671

Complete contact information is available at:
<https://pubs.acs.org/10.1021/acsomega.3c03448>

Notes

The authors declare no competing financial interest.

ACKNOWLEDGMENTS

This material is based upon work supported by the U.S. Department of Energy, Office of Science, under Award Number DE-SC0018598 (design and manufacturing of BN cells and electrochemical measurements), and by the U.S. Department of Energy, Office of Nuclear Energy, under Award Number DE-NE0008751 (X-ray measurements). The authors also acknowledge funding from the Los Alamos National Laboratory under subcontract 22206, through LANL Laboratory Directed Research and Development (LDRD) Project #20210113DR (sample preparations and data analysis). This research used the 8-ID ISS beamline of the National Synchrotron Light Source II, a U.S. Department of Energy (DOE) Office of Science User Facility operated for the DOE Office of Science by Brookhaven National Laboratory under Contract No. DE-SC0012704. We acknowledge useful discussions with Michael F. Simpson (University of Utah) and Haley Williams (UC, Berkeley).

REFERENCES

- (1) Serp, J.; Allibert, M.; Beneš, O.; Delpéch, S.; Feynberg, O.; Ghetta, V.; Heuer, D.; Holcomb, D.; Ignatiev, V.; Kloosterman, J. L.; Luzzi, L.; Merle-Lucotte, E.; Uhlir, J.; Yoshioka, R.; Zhimin, D. The Molten Salt Reactor (MSR) in Generation IV: Overview and Perspectives. *Progress in Nuclear Energy* **2014**, *77*, 308–319.
- (2) Williams, D. F.; Britt, P. F. Technology and Applied R&D Needs for Molten Salt Chemistry. *Technical Report*, 2017.
- (3) Haubenreich, P. N.; Engel, J. R. Experience with the Molten-Salt Reactor Experiment. *Nuclear Applications and Technology* **1970**, *8*, 118–136.
- (4) Mathieu, L.; Heuer, D.; Brissot, R.; Garzenne, C.; Le Brun, C.; Lecarpentier, D.; Liatard, E.; Loiseaux, J. M.; Méplan, O.; Merle-Lucotte, E.; Nuttin, A.; Walle, E.; Wilson, J. The Thorium Molten Salt Reactor: Moving on from the MSBR. *Progress in Nuclear Energy* **2006**, *48*, 664–679.
- (5) Tucker, J. D.; Miller, M. K.; Young, G. A. Assessment of Thermal Embrittlement in Duplex Stainless Steels 2003 and 2205 for Nuclear Power Applications. *Acta Mater.* **2015**, *87*, 15–24.
- (6) Murkute, P.; Oware Sarfo, K.; McGieson, I.; Santala, M. K.; Zhang, Y.; Árnadóttir, L.; Tucker, J. D.; Isgor, O. B. Effect of Thermal Aging on Corrosion Behavior of Duplex Stainless Steels. *SN Applied Sciences* **2022**, *4*, 97.
- (7) Hall, T.; Ahmadi, K.; Radhakrishnan, R.; Snyder, S.; Raiman, S. S. Alloy Plating for Improved Molten Salt Reactor Performance. *ECS Meeting Abstracts* **2020**, MA2020-02, 1189.
- (8) Doyle, P. J.; Koyanagi, T.; Ang, C.; Snead, L.; Mouche, P.; Katoh, Y.; Raiman, S. S. Evaluation of the Effects of Neutron Irradiation on First-Generation Corrosion Mitigation Coatings on SiC for Accident-Tolerant Fuel Cladding. *J. Nucl. Mater.* **2020**, *536*, 152203.
- (9) Raiman, S. S.; Kurley, J. M.; Sulejmanovic, D.; Willoughby, A.; Nelson, S.; Mao, K.; Parish, C. M.; Greenwood, M. S.; Pint, B. A. Corrosion of 316H stainless steel in flowing FLiNaK salt. *J. Nucl. Mater.* **2022**, *561*, 153551.
- (10) Baes, C. F. The Chemistry and Thermodynamics of Molten Salt Reactor Fuels. *J. Nucl. Mater.* **1974**, *51*, 149–162.
- (11) Calderoni, P.; Sharpe, P.; Nishimura, H.; Terai, T. Control of Molten Salt Corrosion of Fusion Structural Materials by Metallic Beryllium. *J. Nucl. Mater.* **2009**, *386–388*, 1102–1106.

- (12) Ding, W.; Bonk, A.; Bauer, T. Corrosion Behavior of Metallic Alloys in Molten Chloride Salts for Thermal Energy Storage in Concentrated Solar Power Plants: A Review. *Frontiers of Chemical Science and Engineering* **2018**, *12*, 564–576.
- (13) Zhang, J.; Forsberg, C. W.; Simpson, M. F.; Guo, S.; Lam, S. T.; Scarlet, R. O.; Carotti, F.; Chan, K. J.; Singh, P. M.; Doniger, W.; Sridharan, K.; Keiser, J. R. Redox Potential Control in Molten Salt Systems for Corrosion Mitigation. *Corros. Sci.* **2018**, *144*, 44–53.
- (14) Newton, M. L.; Hamilton, D. E.; Simpson, M. F. Methods of Redox Control and Measurement in Molten NaCl-CaCl₂-UCl₃. *ECS Trans.* **2020**, *98*, 19.
- (15) Wu, W.; Guo, S.; Zhang, J. Electrochemical Behaviors of Cr(III) in Molten LiF-NaF-KF Eutectic. *Int. J. Electrochem. Sci.* **2018**, *13*, 225–234.
- (16) Doniger, W. H.; Sridharan, K. Application of Voltammetry for Quantitative Analysis of Chromium in Molten 2LiF-BeF₂ (FLiBe) Salt. *J. Electroanal. Chem.* **2019**, *838*, 73–81.
- (17) Zhang, H.; Choi, S.; Zhang, C.; Faulkner, E.; Alnajjar, N.; Okabe, P.; Horvath, D. C.; Simpson, M. F. Square wave voltammetry for real time analysis of minor metal ion concentrations in molten salt reactor fuel. *J. Nucl. Mater.* **2019**, *527*, 151791.
- (18) Leri, A. C.; Hay, M. B.; Lanzirrotti, A.; Rao, W.; Myneni, S. C. Quantitative Determination of Absolute Organohalogen Concentrations in Environmental Samples by X-ray Absorption Spectroscopy. *Anal. Chem.* **2006**, *78*, 5711–5718.
- (19) Leri, A. C.; Ravel, B. Sample Thickness and Quantitative Concentration Measurements in Br K-edge XANES Spectroscopy of Organic Materials. *Journal of Synchrotron Radiation* **2014**, *21*, 623–626.
- (20) Whittenberger, J. D.; Misra, A. K. Identification of Salt–Alloy Combinations for Thermal Energy Storage Applications in Advanced Solar Dynamic Power Systems. *Journal of Materials Engineering* **1987**, *9*, 293–302.
- (21) Grimes, W. R. Molten-Salt Reactor Chemistry. *Nuclear Applications and Technology* **1970**, *8*, 137–155.
- (22) Forsberg, C. W.; Peterson, P. F.; Pickard, P. S. Molten-Salt-Cooled Advanced High-Temperature Reactor for Production of Hydrogen and Electricity. *Nuclear Technology* **2003**, *144*, 289–302.
- (23) Olson, L. C.; Ambrosek, J. W.; Sridharan, K.; Anderson, M. H.; Allen, T. R. Materials Corrosion in Molten LiF–NaF–KF Salt. *J. Fluorine Chem.* **2009**, *130*, 67–73.
- (24) Ludwig, D.; Olson, L.; Sridharan, K.; Anderson, M.; Allen, T. High Temperature Electrochemistry of Molten Fluoride Salt for Measurement of Dissolved Chromium. *Corros. Eng., Sci. Technol.* **2011**, *46*, 360–364.
- (25) Rollet, A.-L.; Bessada, C.; Auger, Y.; Melin, P.; Gailhanou, M.; Thiaudiere, D. A New Cell for High Temperature EXAFS Measurements in Molten Rare Earth Fluorides. *Nuclear Instruments and Methods in Physics Research Section B: Beam Interactions with Materials and Atoms* **2004**, *226*, 447–452.
- (26) Beneš, O.; Konings, R. J. M.; Wurzer, S.; Sierig, M.; Dockendorf, A. A DSC Study of the NaNO₃–KNO₃ System Using an Innovative Encapsulation Technique. *Thermochim. Acta* **2010**, *509*, 62–66.
- (27) Smith, A. L.; Verleg, M. N.; Vlieland, J.; de Haas, D.; Ocádiz-Flores, J. A.; Martin, P.; Rothe, J.; Dardenne, K.; Salanne, M.; Gheribi, A. E.; Capelli, E.; van Eijck, L.; Konings, R. J. M. In Situ High-Temperature EXAFS Measurements on Radioactive and Air-Sensitive Molten Salt Materials. *Journal of Synchrotron Radiation* **2019**, *26*, 124–136.
- (28) MacPherson, H. G. Development of Materials and Systems for the Molten-Salt Reactor Concept. *Reactor Technol.* **1972**, *15*, 136–154.
- (29) Keiser, J. R.; DeVan, J. H.; Lawrence, E. J. Compatibility of Molten Salts with Type 316 Stainless Steel and Lithium. *J. Nucl. Mater.* **1979**, *85–86*, 295–298.
- (30) Koger, J. W. Alloy Compatibility with LiF–BeF₂ Salts Containing ThF₄ and UF₄; 1972, <https://www.osti.gov/biblio/4381831>.
- (31) Koger, J. W. Evaluation of Hastelloy N Alloys after Nine Years Exposure to Both a Molten Fluoride Salt and Air at Temperatures from 700 to 560 °C; 1972, <https://www.osti.gov/biblio/4468052>.
- (32) Ren, W.; Muralidharan, G.; Wilson, D. F.; Holcomb, D. E. Considerations of Alloy N for Fluoride Salt-Cooled High-Temperature Reactor Applications. *ASME 2011 Pressure Vessels and Piping Conference*; 2012; pp 725–736.
- (33) Liu, Y.; Song, Y.; Ai, H.; Shen, M.; Liu, H.; Zhao, S.; Liu, Y.; Fei, Z.; Fu, X.; Cheng, J. Corrosion of Cr in Molten Salts with Different Fluoroacidity in the Presence of CrF₃. *Corros. Sci.* **2020**, *169*, 108636.
- (34) Choi, S.; Strianese, A. R.; Simpson, M. F. Electrochemical Techniques to Monitor the Concentration of Oxide in Molten FLiNaK Salt. *ECS Meeting Abstracts* **2020**, *MA2020-02*, 2922–2922.
- (35) Consiglio, A. N.; Carotti, F.; Liu, E.; Williams, H.; Scarlet, R. O. Design and Operation of a Molten Salt Electrochemical Cell. *MethodsX* **2022**, *9*, 101626.
- (36) Delpéch, S.; Cabet, C.; Slim, C.; Picard, G. S. Molten Fluorides for Nuclear Applications. *Mater. Today* **2010**, *13*, 34–41.
- (37) Khokhlov, V.; Ignatiev, V.; Afonichkin, V. Evaluating Physical Properties of Molten Salt Reactor Fluoride Mixtures. *J. Fluorine Chem.* **2009**, *130*, 30–37.
- (38) Pint, B. A.; Su, Y.-F.; Sulejmanovic, D.; Pillai, R. Characterization of Fe and Cr Dissolution and Reaction Product Formation in Molten Chloride Salts With and Without Impurities. *Materials at High Temperatures* **2023**, *0*, 1–11.
- (39) Leshchev, D.; Rakitin, M.; Luvizotto, B.; Kadyrov, R.; Ravel, B.; Attenkofer, K.; Stavitski, E. The Inner Shell Spectroscopy Beamline at NSLS-II: A Facility for in Situ and Operando X-ray Absorption Spectroscopy for Materials Research. *Journal of Synchrotron Radiation* **2022**, *29*, 1095–1106.
- (40) Ravel, B.; Newville, M. ATHENA, ARTEMIS, HEPHAESTUS: Data Analysis for X-ray Absorption Spectroscopy Using IFEFFIT. *Journal of Synchrotron Radiation* **2005**, *12*, 537–541.
- (41) Newville, M. Larch: An Analysis Package for XAFS and Related Spectroscopies. *Journal of Physics: Conference Series* **2013**, *430*, 012007.
- (42) Liu, X. Formation of Three-Dimensional Bicontinuous Structures via Molten Salt Dealloying Studied in Real-Time by in Situ Synchrotron X-ray Nano-Tomography. *Nat. Commun.* **2021**, DOI: 10.1038/s41467-021-23598-8.
- (43) Dias, E. T.; Gill, S. K.; Liu, Y.; Halstenberg, P.; Dai, S.; Huang, J.; Mausz, J.; Gakhar, R.; Phillips, W. C.; Mahurin, S.; Pimblott, S. M.; Wishart, J. F.; Frenkel, A. I. Radiation-Assisted Formation of Metal Nanoparticles in Molten Salts. *J. Phys. Chem. Lett.* **2021**, *12*, 157–164.
- (44) Dias, E. T.; Gill, S. K.; Liu, Y.; Halstenberg, P.; Dai, S.; Huang, J.; Mausz, J.; Gakhar, R.; Phillips, W. C.; Mahurin, S.; Pimblott, S. M.; Wishart, J. F.; Frenkel, A. I. Correction to “Radiation-Assisted Formation of Metal Nanoparticles in Molten Salts. *J. Phys. Chem. Lett.* **2021**, *12*, 1777–1777.
- (45) Ronne, A.; He, L.; Dolzhenkov, D.; Xie, Y.; Ge, M.; Halstenberg, P.; Wang, Y.; Manard, B. T.; Xiao, X.; Lee, W.-K.; Sasaki, K.; Dai, S.; Mahurin, S. M.; Chen-Wiegart, Y.-c. K. Revealing 3D Morphological and Chemical Evolution Mechanisms of Metals in Molten Salt by Multimodal Microscopy. *ACS Appl. Mater. Interfaces* **2020**, *12*, 17321–17333.
- (46) Bawane, K.; Liu, X.; Gakhar, R.; Woods, M.; Ge, M.; Xiao, X.; Lee, W.-K.; Halstenberg, P.; Dai, S.; Mahurin, S.; Pimblott, S. M.; Wishart, J. F.; Chen-Wiegart, Y.-c. K.; He, L. Visualizing Time-Dependent Microstructural and Chemical Evolution during Molten Salt Corrosion of Ni-20Cr Model Alloy Using Correlative Quasi in Situ TEM and in Situ Synchrotron X-ray Nano-Tomography. *Corros. Sci.* **2022**, *195*, 109962.